

# STUDY OF PHYSICAL PROCESSES AFFECTING THE TRANSFORMATION OF COLD AIR OVER LAND AFTER OUTBREAK OF COLD WAVES IN EAST ASIA

Zhao Qiang (赵 强)

National Research Center for Marine Environment Forecasts, State Oceanic Administration, Beijing 100081

and Ding Yihui (丁一汇)

Chinese Academy of Meteorological Sciences, Beijing 100081

Received July 18, 1991

## ABSTRACT

Authors have studied the transformation processes of cold air over land in East Asia for eight cases which occurred in different months of 1981. First, the surface eddy sensible and latent heat fluxes, and drag coefficient were estimated according to the approach of similarity theory. Then, the apparent heat source, the apparent moisture sink, and solar and long-wave radiative heating (or cooling) were further calculated through the budget method and physical parameterization algorithm. It has been found that the cold air immediately starts the transformation process over land once it moves away from its region of origin. In winter, the degree of transformation of cold air mass gradually intensified as it travelled southeastward; while arriving in the ocean, the cold air mass underwent the most significant transformation process. In summer, the most vigorous transformation of thermal and moisture fields was observed in North China and Mongolian region, with much greater intensity than that in winter.

**Key words:** cold air, air mass transformation, land-atmosphere interaction, diagnostic analysis

## I. INTRODUCTION

The Siberian high is a kind of cold high that is situated in the central and eastern part of Siberia and North Mongolia. As the cold high moves from its source area to the East Asian continent and the western part of the Pacific Ocean, the dry cold polar air is gradually modified by the new underlying surface. In the wintertime, the modification over the East China Sea is remarkable due to intense sensible and latent heat supplies. This problem was extensively studied by many authors during the air mass transformation experiments (AMTEX) that were conducted in 1974 and 1975 (AMTEX '74 and AMTEX '75). The results of the two extensive experiments indicated that total amount of sensible and latent heat supplies from the Kuroshio current to the atmosphere reaches  $800 \text{ W m}^{-2}$  during the cold air outbreaks, while in the other time the amount is about  $170 \text{ W m}^{-2}$  only (Lenchow and Agee, 1976; Nitta and So, 1980). It is clear that in winter the cold air transformation processes over the sea surface are very intense. However, the cold air transformation processes over the East Asian continent were not studied during the two experiments. By using composite method for 19 cases of strong Siberian highs that were selected from data sets covering 5 winters (1980—1984), Ding and Krishnamurti (1987) indicated that the transformation processes start actually over the continent, that the intensity of the modification over the continent is about one third or one fourth of that over the

ocean and that the modification processes can be divided into different stages. However, their results were mainly obtained from residual calculation by using heat budget equation. They did not calculate turbulent processes directly and did not discuss the condition in other seasons. So the structure and the transformation of the cold air in summer or in other seasons are not very clear yet.

The objective of the present paper is, based on previous studies, aimed to calculate directly turbulent transfer of sensible and latent heat and other diabatic heating (cooling) processes of cold highs at different stages and in different seasons of a year in order to make a thorough and careful study of the transformation of the cold air over the continent after its moving southwards from its source area. This is very useful to understand the variation of intensity and the thermodynamic characteristics of the cold air or the cold high.

## II. THE SELECTION OF CASES AND DATA

Siberia is the region of most significant high activity. In order to study the processes of generation, development and transformation of dry and cold Siberian highs, cases could be selected following the highest pressure values of their centers. Ding and Krishnamurti(1987) followed the same criterion in their work. In addition to high intensity, we also consider the representativeness of high tracks. According to the statistics of 101 cases of cold highs during 1980—1984 by Ding and Krishnamurti, the cold highs tend to move along three main tracks (see Fig. 1). Among them, the first track, called northwest track, is the most frequently observed one and accounts for about 64% of the total tracks.

In the present study, all 8 selected cases moved along the northwest track. In order to make a comparison between characteristics of cold highs in different seasons, we selected almost the same number of cases in each season for analysis. Because the surface pressure at the center of cold high varies greatly from one season to another, the criterion used in selecting cases should be correspondingly changed in different seasons. Generally, cases that be picked out in this study all have the highest pressure at the center in the corresponding seasons (see Table 1).

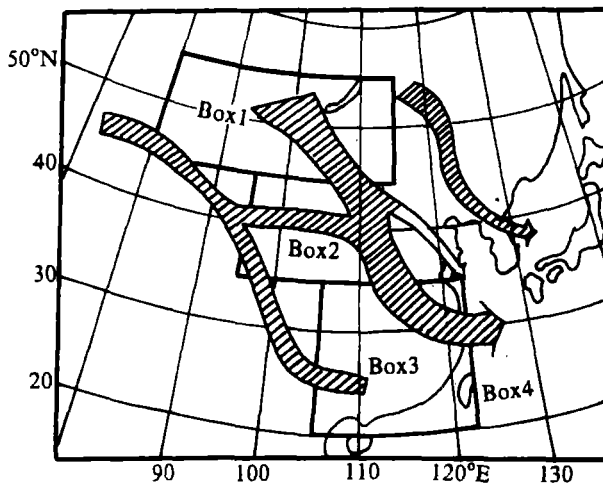


Fig. 1. Schematic map of tracks of the Siberian high and division of the region under study (after Ding and Krishnamurti, 1987).

**Table 1.** The Selected 8 Cases of Cold Highs in 1981

Cases	Period	Maximum central pressure (hPa)
1	Jan. 18—29	1085
2	Feb. 23—28	1055
3	March 22—28	1045
4	May 1—5	1045
5	June 15—18	1015
6	Aug. 3—6	1025
7	Sep. 25—30	1030
8	Nov. 29—Dec. 4	1060

We used the regional composite method in which four different stages of these southward moving cold highs are represented by four different regions so as to investigate distinctive feature of cold high in each phase of its life cycle. Among the four regions (boxes), the first (Box 1) is Siberia and North Mongolia ( $80^{\circ}$ — $115^{\circ}$ E,  $45^{\circ}$ — $55^{\circ}$ N); the second one (Box 2) is the northern part of China ( $95^{\circ}$ — $130^{\circ}$ E,  $35^{\circ}$ — $50^{\circ}$ N); the third one (Box 3) is central and South China ( $105^{\circ}$ — $122^{\circ}$ E,  $20^{\circ}$ — $35^{\circ}$ N); and the last one (Box 4) is over the sea region ( $122^{\circ}$ — $145^{\circ}$ E,  $20^{\circ}$ — $40^{\circ}$ N) (see Fig. 1). In most of cases, the cold highs moved through all boxes in order of time. But, some of cases (mainly in summer), affected by seasons, were modified thoroughly and disappeared over land without passing through all the boxes. So the result for later stage of composite cold high activity is less representative in some degree.

The dataset in our study is composed of conventional observations, which include two upper-air observations and four surface observations on daily basis, at several stations in the vicinity of the high center. The upper-air observations contain 11 levels: surface, 1000, 850, 700, 500, 400, 300, 250, 200, 150 and 100 hPa. The meteorological elements are temperature, depression of the dew point, wind speed and direction. Moreover, temperature and dew point temperature at significant levels and wind speed direction at maximum wind levels are available. The surface observation includes sea-level pressure, temperature, relative humidity, wind speed, wind direction, and 0 cm soil temperature. It is unfortunate that data outside China at the significant levels, maximum wind levels and 0 cm soil level are unavailable. Upper-air and surface observations inside the country were obtained from "Monthly Aerological Bulletin of China" and "Monthly Surface Bulletin of China" published by Data Department of Beijing Meteorological Center. The data at significant levels, wind levels and 0 cm soil level were copied down from original station reports collected by the Center. Data outside the country were selected from tape files kept by the same Center.

### III. DATA PROCESSING AND COMPUTATIONAL ASPECT

To consider terrain effect and to describe the element distributions and physical processes in the boundary layer in detail, we adopt a  $\sigma$  coordinate system. We interpolate the data into 19 different levels with the same pressure difference, about 50 hPa, between two neighbouring levels. After coordinate transformation from  $p$ -system to  $\sigma$ -system, computation may be carried on at the constant  $\sigma$  surface. The coordinate transformation formula is

$$\sigma = \frac{P - P_t}{P_s - P_t}, \quad (1)$$

where  $P$  is the pressure at the computational level,  $P_t$  is the pressure at the top level, 100 hPa in this paper, and  $P_s$  is the surface pressure.

The similarity theory is used in calculating sensible and latent heat flux near the surface. We used basically the scheme suggested by Louis (1979). The drag coefficients of momentum and heat turbulent exchange are respectively

$$C_m = \left[ \frac{k^2}{\ln(z/z_0)} \right] F_m, \tag{2}$$

$$C_h = \frac{1}{R} \left[ \frac{k^2}{\ln(z/z_0)} \right] F_h, \tag{3}$$

where  $k$  is Von Karman constant,  $z$  is the height of top level of surface layer, taken to be 10 m (the height of weather vane),  $z_0$  is the height of roughness, assumed to be 0.1 m, and  $R$  is the ratio of momentum drag coefficient to heat drag coefficient for neutral stability and its value was estimated 0.74 by Businger (1971).  $F_m$  and  $F_h$  are affecting factors of stability on drag coefficients and were given in general form with using data fitting method by Louis:

$$F = \begin{cases} 1 - \frac{b \cdot Ri_b}{1 + c \cdot |Ri_b|^{1/2}}, & \text{unstable} \\ \frac{1}{(1 + b' \cdot Ri_b)^2}. & \text{stable} \end{cases} \tag{4}$$

$$Ri_b = gz \cdot \frac{\theta(z) - \theta(z_0)}{\overline{\theta u}^2} \tag{5}$$

is bulk Richardson number.  $b = 2b' = 9.4$  and  $c = c^* a^2 b(z/z_0)^{1/2}$ , where  $c^* = 7.4$  for momentum and  $c^* = 5.3$  for heat and moisture,  $a^2 = k^2 / [\ln(z/z_0)]$ . The expression of  $a^2$  is the momentum drag coefficient for neutral stability with the same form as that in the brackets of formula (2) or (3).

The formula of upward turbulent sensible heat flux from the surface is

$$f_h = \rho_s C_h C_p (T_{z_0} - T_s) \cdot |\mathbf{V}_s|, \tag{6}$$

and turbulent latent heat flux is

$$f_q = \rho_s C_h L (q_{z_0} - q_s) \cdot |\mathbf{V}_s|, \tag{7}$$

where  $\rho_s$ ,  $T_s$ ,  $\mathbf{V}_s$ ,  $q_s$  are air density near the surface, and temperature, wind speed and specific humidity at the top of surface layer, respectively.  $T_{z_0}$  is the temperature at the top of laminar layer  $z_0$  which is also called surface roughness height.  $T_{z_0}$  can be drawn from soil temperature by using iteration method in which the following relationship is used (6):

$$T_{z_0} = T_G + 0.00962 \frac{\theta^*}{k} \left( \frac{\mu^* z_0}{\nu} \right)^{0.45}, \tag{8}$$

where  $\nu$  is coefficient of kinematic viscosity (assumed to be  $1.5 \times 10^{-5} \text{m}^2 \text{s}^{-1}$ ),

$$\begin{cases} u^* = \sqrt{|w'u'|} \\ \theta^* = -\frac{w'\theta'}{u^*} \end{cases} \quad (10)$$

are characteristic velocity and characteristic temperature of turbulent process.  $q_{z_0}$  is the humidity at  $z_0$ ,

$$q_{z_0} = q_{\text{sat}}(T_{z_0}) \cdot RH, \quad (11)$$

where  $q_{\text{sat}}(T_{z_0})$  is saturation specific humidity when temperature is  $T_{z_0}$  and  $RH$  is relative humidity at  $z_0$  determined by the relative humidity at the height of instrument screen and the characteristics of surface turbulence.

Above the surface layer, turbulent flux is estimated as diffusive flux. Diffusion coefficient  $K$  is determined by height, vertical wind shear, atmospheric stability and mixing length (1):

$$K_m = l^2 \left| \frac{\Delta V}{\Delta z} \right| F. \quad (12)$$

The heat diffusion coefficient  $K_h$  has a similar form. The mixing length is introduced as an asymptotic form:

$$l = \frac{kz}{1 + k \cdot z / \lambda}, \quad (13)$$

where the asymptotic mixing length  $\lambda$  is an adjustable parameter, 100 m in the present study.  $F$  in (12) has the same form as in (4) or (5), but the Richardson number and coefficient  $C$  need to be redefined as  $g\Delta z\Delta\theta / \bar{\theta}\Delta V^2$  and  $c^* l^2 b[(z + \Delta z / z)^{1/3} - 1]^{3/2} / (z^{1/2} \Delta z^{3/2})$ .

The parameterization scheme in calculating radiative flux is same as that used by Ding and Krishnamurti. The four main parts of this scheme are: (1) specification of form and fraction of cloud, based on threshold value of relative humidity, (2) estimation of longwave radiation by emissivity, (3) estimation of shortwave radiation, and (4) surface energy balance. Detailed description can be found in reference (Ding, 1987).

The budget equations of apparent heat source and apparent moist sink are deduced from thermodynamic equation and moisture equation in sigma coordinate:

$$\begin{aligned} \overline{P^* Q_1} &\equiv C_p \left[ \frac{\partial \overline{P^* T}}{\partial t} + \nabla \cdot \overline{P^* \nabla T} + \frac{\partial \overline{P^* \sigma T}}{\partial \sigma} - \frac{RT\bar{\omega}}{C_p(\sigma + P_t / P^*)} \right] \\ &= Q_R + LP^* \overline{C^*} - C_p \frac{\partial \overline{P^* \sigma' T'}}{\partial \sigma} + \frac{RT'\bar{\omega}'}{\sigma + P_t / P^*}, \end{aligned} \quad (14)$$

$$\begin{aligned} \overline{P^* Q_2} &\equiv -L \left[ \frac{\partial \overline{P^* q}}{\partial t} + \nabla \cdot \overline{P^* \nabla q} + \frac{\partial \overline{P^* \sigma q}}{\partial \sigma} \right] \\ &= LP^* \overline{C^*} - \frac{\partial \overline{P^* \sigma' q'}}{\partial \sigma}, \end{aligned} \quad (15)$$

where  $Q_R$  is term of radiation heating (cooling),  $C^*$  is net water condensation and  $P^*$  is defined as

$$P^* = P_s - P_t. \quad (16)$$

The areal average and its horizontal derivative of the terms in Eq. (15) could be obtained by curved surface fitting method that means meteorological variable  $A$  is expanded as a linear function:

$$A = a_0 + a_1 X + a_2 Y, \quad (17)$$

where  $(X, Y)$  is the coordinates relative to the geometric center of fitted points.  $a_0$ ,  $a_1$  and  $a_2$  are evaluated by least square method. So, we may obtain

$$\bar{A} = a_0, \quad \frac{\partial \bar{A}}{\partial x} = a_1, \quad \frac{\partial \bar{A}}{\partial y} = a_2. \quad (18)$$

#### IV. GENERAL STRUCTURES OF SIBERIAN HIGH COLD MASS AND VERTICAL TRANSPORTS

To compare the characteristics of cold air transformation in different seasons, we divide the 8 cases into two groups (in winter half year and in summer half year). One includes cases 1, 2, 3, 8 (Jan., Feb., March, Dec.) and the other has cases 4, 5, 6, 7 (May, June, Aug., Sep.).

The temperature structure of cold high in winter (Fig. 2a) indicates that there is a strong inversion (below 800 hPa) in early days of development of cold air. As cold air moves southward, the inversion gets weaker and disappears finally. In North China (Box 2) it is unseen already. After moving to Box 3, only a new weak inversion or isothermal layer occurs in the middle troposphere. According to Ding and Krishnamurti, the main causes of the former inversion are due to strong longwave radiation cooling and downdrafts near the surface and for the latter the subsidence heating is important. Accompanying evolution of inversion, in the full depth of troposphere, especially in its lower part, temperature becomes higher and deep polar cold air mass is transformed into warmer air mass gradually. Near the surface temperature goes up by 30°C and 20°C for the upper troposphere. The evolution of moisture structure (Fig. 2b) is similar to that of temperature structure. The specific humidity increases rapidly as cold high moves southward, especially in the middle and lower part of troposphere. It is indicated that cold air undergoes the moisture transformation at same time when it modifies its temperature. It is worth noting that humidity increase below 700 hPa is obvious from Box 2 to Box 3 and is comparable with that over the ocean. It shows that moisture transformation over land is also remarkable.

The temperature structure of the cold high in summer has two obvious differences from those in winter. At first the inversion does not exist. Secondly, the strongest heating appears in Box 2 and on the contrary the temperature has a drop as transformed air mass moved to the oceanic area (Fig. 3). This kind of evolution of temperature structure is closely related to land-sea contrast of temperature. In summer the temperature is lower on land than on the sea surface, so it has an opposite impact on temperature stratification as compared with that in winter. The area where humidity in cold air increases most rapidly is also North China. As the cold high shifts to the sea surface, its humidity reduced remarkably (Figure is omitted). It is indicated that the structures of temperature and humidity over sea are evidently different from those over land. Generally, cold air is much warmer and wetter over land than over sea. It is justly opposite to the situation in winter.

Calculation of vertical velocity indicates that relatively strong downdraft is maintained in full depth of troposphere as cold air undergoes transformation process during southward travelling in different seasons. The maximum value appears near 550 hPa over North China. When

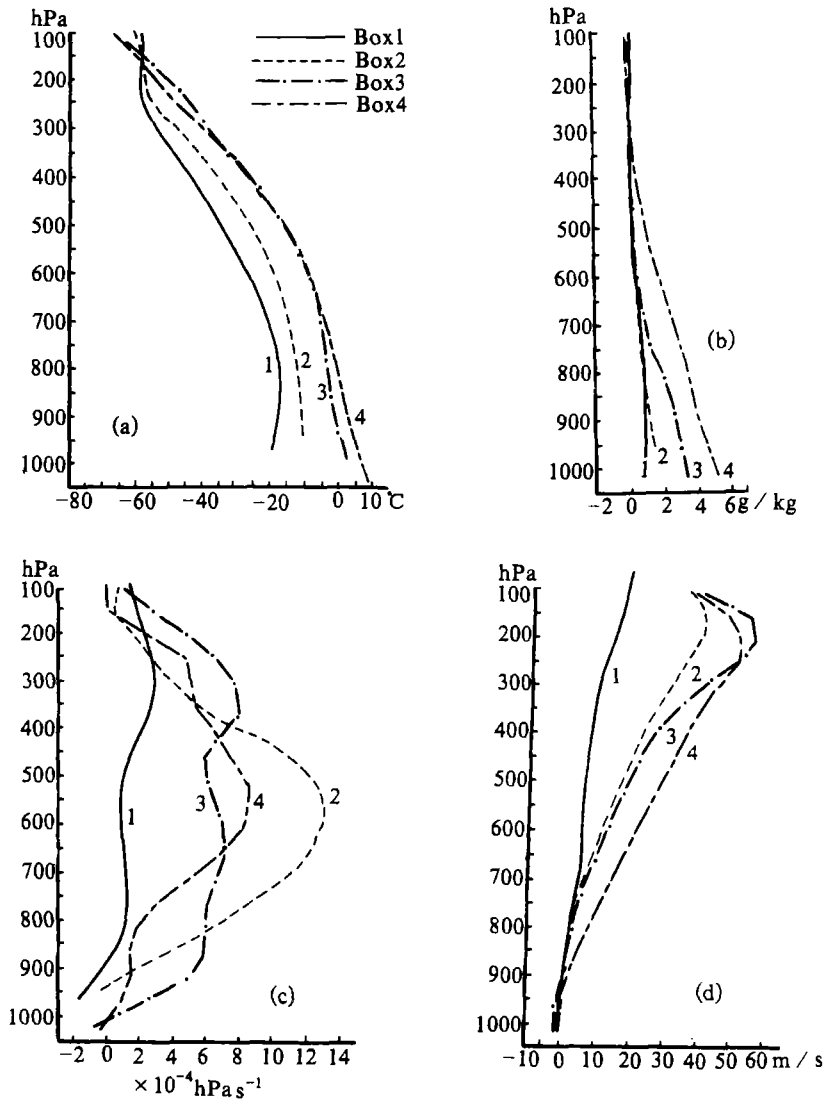


Fig. 2. Basic structure of cold high at different stages in winter. (a) temperature ( $^{\circ}\text{C}$ ), (b) specific humidity ( $\text{g}/\text{kg}$ ), (c) vertical velocity  $\omega$  ( $\times 10^{-4} \text{ hPa}/\text{s}$ ), and (d) zonal wind ( $\text{m}/\text{s}$ ).

cold high moved southward to the central and South China and oceanic area, the downdraft weakened. So the strongest downdraft exists at early stages. The distribution of vertical velocity in winter is given (Fig. 2c).

Fig. 2d is mean profiles of zonal wind in winter. A similar distribution appears in summer (figure is omitted). It is obvious that upper-level west wind is enhanced gradually in winter or in summer. In winter, upper-level west wind which is weak in source area grows in strength continuously after outbreak of cold air and reaches the maximum value, about  $55 \text{ m}/\text{s}$  at 200 hPa, in Box 3. In summer, the upper west wind in Box 1 is relatively strong. Then they are

strengthened consistently and reach the maximum value (about 50 m/s) in Box 4. So, when cold air moves to Box 3 or Box 4 it is located just below the upper westerly jet.

Above observational analysis of cold high suggests that cold air experiences some remarkable transformation no matter what season. Among the physical processes which result in transformation, the heating or cooling from the underlying surface is an important factor. So the computed results of surface sensible heat flux and moisture flux at different stages will be discussed in the first place.

Following the similarity theory, we have computed the upward turbulent sensible heat and latent heat (moisture) fluxes from surface. For data limitation, calculations are not taken in the regions outside China (Boxes 1 and 4 mainly). Inside the country, we collect and use the four observation time surface observational data. These data make it possible that we understand the characteristics of diurnal variation of sensible and latent heat fluxes.

Table 2. Land-Air Sensible, Latent and Total Heat Flux ( $W m^{-2}$ ) and Bowen Ratio of 8 Cases of Outbreaks of the Cold Air in 1981

		Cases								Winter mean	Summer mean
		1	2	3	4	5	6	7	8		
Sensible heat flux	Box 2	67	72	66	173	170	77	74	23	57	124
	Box 3	35	49	55	90	/	63	47	57	49	67
Latent heat flux	Box 2	14	16	33	60	256	136	58	9	18	127
	Box 3	35	12	60	86	/	148	80	34	35	105
Total heat flux	Box 2	81	88	99	233	426	213	132	32	75	251
	Box 3	70	61	115	176	/	211	127	91	84	172
Bowen ratio	Box 2	4.8	4.5	2.0	2.9	0.66	0.55	1.3	2.6	3.2	1.0
	Box 3	1.0	4.1	0.92	1.0	/	0.42	0.59	1.7	1.4	0.64

The land-air turbulent heat fluxes given in Table 2 show that the heat fluxes in cold air processes are both directed from the surface to the atmosphere in winter and in summer. So it is indicated that the cold air begins to be heated by the underlying surface and to experience the transformation just after it moves away from its source area and moves southward. By making a comparison between cases in winter and in summer, we can see that the sensible and latent heat transport in latter cases is obviously by 2-3 times greater than that in former cases. It shows that the turbulent exchange processes occurring in lower layer of southward moving cold air in summer are more violent and this partly explains why in summer the cold highs are often modified rapidly and disappear on land and only a few of them can move further to South China or to the sea area. The calculated Bowen ratios demonstrate that sensible heating is a primary factor in land transformation process of winter cold air. And in summer, latent heat transport is as much as or greater than the sensible heat transport. It is indicated that the latent heating plays an important part in land transformation process of cold air. This is due to less soil moisture in winter and greater soil moisture in summer. The heating near the surface also varies in different regions. It can be seen from comparison between situations in Boxes 2 and 3 that in winter total heat flux in Box 3 is slightly stronger than that in Box 2,  $84 W m^{-2}$  and  $75 W m^{-2}$  respectively, and in summer mean total heat flux in Box 2 is  $251 W m^{-2}$  that is much greater than

$172 \text{ W m}^{-2}$  in Box 3. This indicated that the strongest transforming region is changeable in different seasons, which is located in South China or over ocean in winter and in North China or farther north area in summer.

**Table 3.** Land–Air Sensible, Latent and Total Heat Flux ( $\text{W m}^{-2}$ ) and Bowen Ratio of Cold Air Activities in Different Boxes

		Winter half year				Summer half year			
		mean				mean			
		Beijing Time				Beijing Time			
		02	08	14	20	02	08	14	20
Sensible heat flux	Box 2	-18	-6	266	-12	-22	61	454	1
	Box 3	-7	9	203	-8	10	32	218	7
Latent heat flux	Box 2	-3	-1	78	-3	-12	72	448	2
	Box 3	-6	5	148	-7	21	54	328	17
Total heat flux	Box 2	-21	-7	344	-15	-34	133	902	3
	Box 3	-13	14	351	-15	31	86	546	24
Bowen ratio	Box 2	6.0	6.0	3.4	4.0	1.8	0.8	1.0	0.5
	Box 3	1.2	1.8	1.4	1.1	0.5	0.6	0.7	0.4

**Table 4.** Surface Momentum Drag Coefficient  $C_m$ , Heat Drag Coefficient  $C_h$ , Land–Air Temperature Difference  $T_g - T_a$  ( $^{\circ}\text{C}$ ) and Bulk Richardson Number  $Ri_b$

		Average for winter half year					Average for summer half year				
		Beijing Time					Beijing Time				
		02	08	14	20	mean	02	08	14	20	mean
$C_m$	Box 2	3.2	3.8	11.6	3.2	5.5	3.2	8.5	10.0	4.5	6.6
	Box 3	4.8	6.2	8.2	4.4	5.9	6.0	7.7	10.7	6.4	7.7
$C_h$	Box 2	4.3	5.2	17.8	4.5	7.9	4.4	12.6	15.0	6.2	9.6
	Box 3	6.5	8.6	11.7	6.1	8.2	8.4	10.9	15.1	10.4	11.2
$T_g - T_a$	Box 2	-2.5	-1.4	10.6	-2.6	1.0	-2.1	2.8	15.5	-0.8	3.8
	Box 3	-0.8	0.4	7.4	-1.0	1.5	0.4	1.8	9.1	0.3	2.9
$Ri_b$	Box 2	0.38	0.29	-0.54	0.50	0.16	0.29	-0.16	-0.34	0.18	-0.01
	Box 3	0.11	-0.0	-0.13	0.12	0.02	0.06	-0.10	-0.33	-0.04	-0.10

In Table 2 daily mean fluxes are given, while in Table 3 corresponding values at different time are given. From Table 3 it can be seen that turbulent activities near surface have obvious diurnal variation. The most violent turbulence occurs at 14 Beijing Time (BT) among 4 observation times. The mean total heat flux at 14 BT in Box 2 of four summer cases reaches  $902 \text{ W m}^{-2}$ , while at other 3 times the mean heat flux are much weaker or even directed downward (from air to land). The maximum value of surface turbulent heat flux for winter cases (at 14 BT) is less than that for summer cases and total heat flux in Box 2 ( $344 \text{ W m}^{-2}$ ) is only as  $1/3$  time as corresponding value in summer. It is notable that in summer transports at 8 BT in Boxes 2 and 3 are both upward while in winter the transport in Box 2 is downward which may be related to

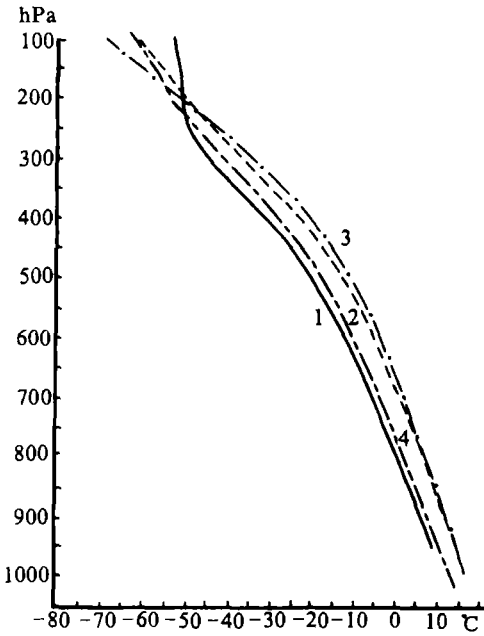


Fig.3. Temperature distribution of cold high at different stages in summer.

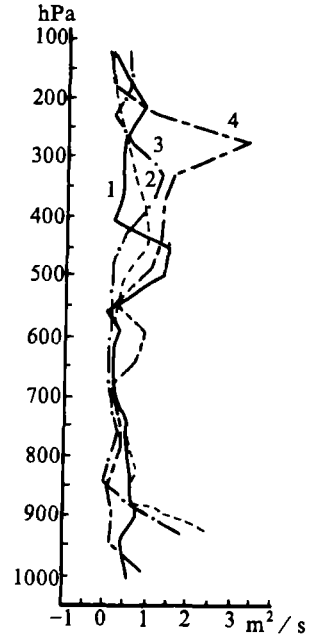


Fig.4. Turbulent diffusion coefficients in cold highs ( $m^2 s^{-1}$ ) for winter half year.

existence and persistence of nocturnal inversion.

It is shown by calculations that surface momentum drag coefficient is remarkable in diurnal variation (see Table 4). The maximum value reaches up to  $11.6 \times 10^{-3}$  which occurs at 14 BT and the minimum value is only  $3.2 \times 10^{-3}$  which occurs at night (02 or 20 BT). There is about three-fold difference between two values. Heat drag coefficient has a similar diurnal variation, but with greater value. In winter drag coefficients in Boxes 2 and 3 are  $5.5 \times 10^{-3}$  and  $5.9 \times 10^{-3}$ , respectively, and in summer they are  $6.6 \times 10^{-3}$  and  $7.7 \times 10^{-3}$ , greater than the values in winter. All of them are much larger than  $C_m$  used in sea area ( $1-2 \times 10^{-3}$ ), also larger than the mean value generally used on land in the past (about  $3 \times 10^{-3}$ ). Over the Tibetan Plateau, Yeh and Gao et al. (1981) assumed  $C_m = 8 \times 10^{-3}$  for their computation of surface heat flux. The result obtained from the measurements in 1986 summer Qinghai-Xizang Plateau expedition suggested  $C_m = 5-6 \times 10^{-3}$ <sup>(1)</sup> which is close to values obtained in this paper. From the above analysis, it can be seen that only daily mean data or observations at 08 BT and 20 BT are inadequate for computing heat exchange processes. The thus-obtained results may even give a misunderstanding.

The turbulent diffusion coefficients calculated from twice daily radiowind data, are given in Fig. 4. Generally, there are two strong turbulent activity layers from surface to 100 hPa. One exists in the lower troposphere and the other is located in upper part and near top of the troposphere. In the lower boundary, the effect of turbulence activity goes only up to 800 hPa in

(1) Ma Shufen et al.(1988), The preliminary calculation of surface turbulent heat flux during Qinghai-Xizang Plateau expedition in 1986 summer.

winter, but in summer, much stronger turbulence may extend up to 600 hPa. The intensity of turbulence in upper part and near top of the troposphere is changeable as season and geographic location change. Many studies have shown that the turbulent activity in upper part and near top of troposphere has close relationship to upper air jet (Shapiro, 1976).

#### V. HEAT BALANCE DURING SOUTHWARD OUTBREAKS OF THE COLD AIR

Calculation of apparent heat source  $Q_1$  (Fig.5) indicates that cold air in full depth of the troposphere is heat sink in its source area in winter, so the air inside cold high has deep cooling layer. Mean cooling rate reaches 3—4 °C/d from 800—300 hPa. When cold air moves to Box 2, warming appears in the upper part of the troposphere and the lower boundary layer. Heating rate for the latter is about 2 °C/d and for the upper part of the troposphere this heating rate reaches up to 8 °C/d (in the vicinity of 200 hPa). Ding and Krishnamurti (1987) have explained the strong upper level eddy sensible heating in the neighbourhood of jet at high latitudes in winter by using aircraft soundings in North America. They pointed out that this heating is the result of heat convergence created by strong turbulence exchange in jet region. The distribution of apparent heat source implies that cold air actually underwent temperature transformation. In Box 3, heating rate in the lower boundary is enhanced which suggests increase in temperature transformation caused by the underlying surface. When the cold air continuously moves to oceanic region the heating effect of the warm sea surface on lower part of cold air is more significant. The heating rate is 3 °C/d and the depth of the heated layer increased by about 50 hPa.

Unlike the situation in winter, summer cold air in Box 1 has the full depth of the troposphere heated. The strongest heating, which appears near the surface and in the lower troposphere, reaches 6 °C/d. This suggests that the central and East Siberia and Mongolia should not be called as source area of cold air in summer, because cold air has had an obvious transformation process already here. This can also explain why cold air in summer is difficult to

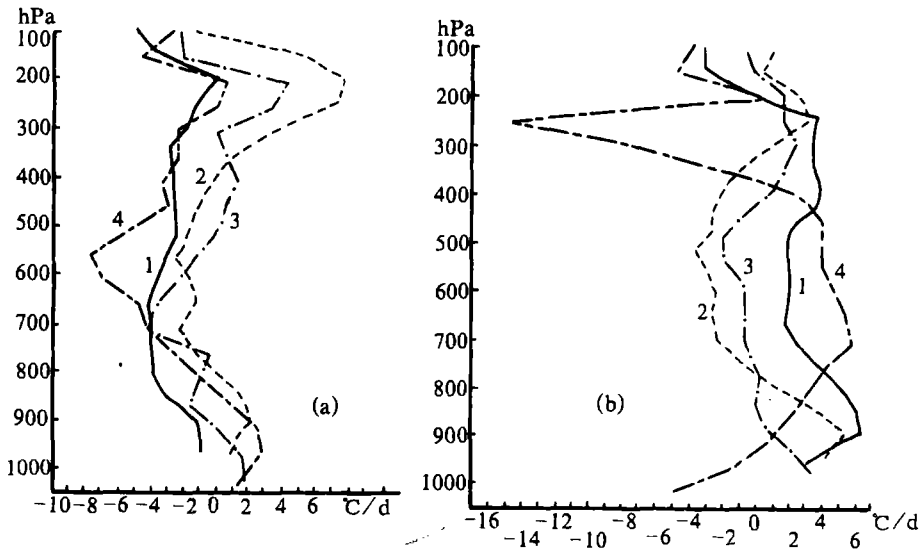


Fig. 5. The vertical distribution of apparent heat source  $Q_1$  ( $^{\circ}\text{C}/\text{d}$ ) for winter half year (a) and summer half year (b).

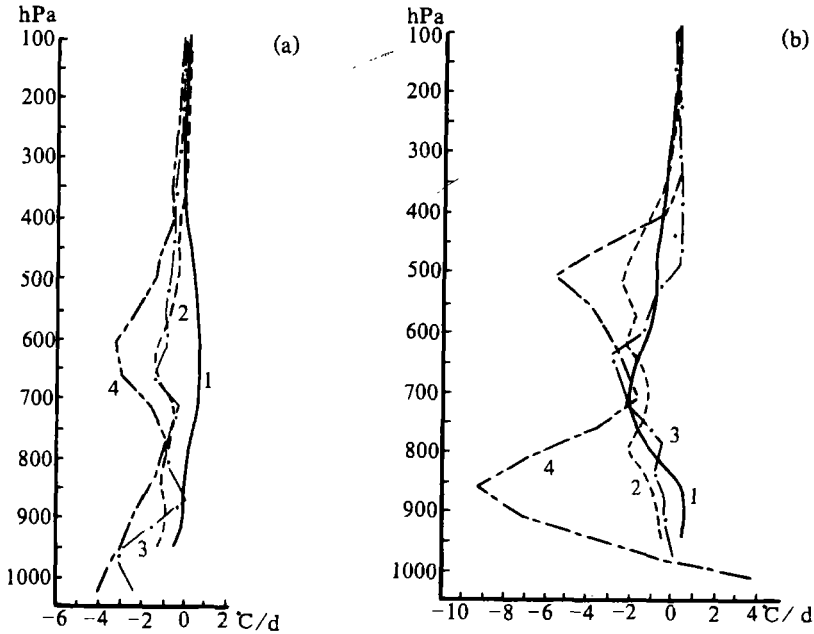


Fig. 6. The vertical distribution of apparent moist sink  $Q_2$  ( $^{\circ}\text{C} / \text{d}$ ) for winter half year (a) and summer half year (b).

develop into very strong one. Another interesting phenomenon is that the heating rate in the lower layer decreases continuously as summer cold air moves from Boxes 1 to 2 and 3. It implies that the turbulence activity in the interface layer of land-air has weakened which is in agreement with the results calculated for sensible heat turbulent exchange in the previous section. The distribution of  $Q_1$  in Box 4 that shows heating in middle layer and cooling in upper and lower layers is out-of-phase in comparison with ones at earlier stages. The cooling appears in the lower layer of summer cold air because the sea surface is no longer a warmer, but colder underlying surface, so that the cold air losses its heat to ocean when it migrates to the oceanic region.

The distribution of apparent moisture sink  $Q_2$  in the cold air is given in Fig. 6. In winter, except for slight increase near the surface (about 850 hPa), which is mainly related to the evaporation of cloud droplet, moisture of cold air in source area decreases in the middle and lower troposphere. It reflects the existence of condensation or congelation process in source area that has something to do with the middle-low cloud in this area. When the cold air moves to Box 2, moisture in the full depth of the troposphere increases. This kind of moisture increase, mainly created by evaporation process, may has some links with the strong downdraft of cold air in its southward course. The distributions similar to Box 2 are found in Boxes 3 and 4 except larger magnitudes of moisture increase. In latter two areas, the ground evaporation may be a main factor due to relatively moist underlying surface. However, the most increase of moisture arises over the warm moist sea surface where the upward transport of moisture (expressed in form of latent heating) reaches  $4^{\circ}\text{C} / \text{d}$ .

In summer, similar to  $Q_1$  profile showing, the transformation process of moisture in cold air has already existed in Box 1. The moisture increase appears in the layer above 850 hPa and

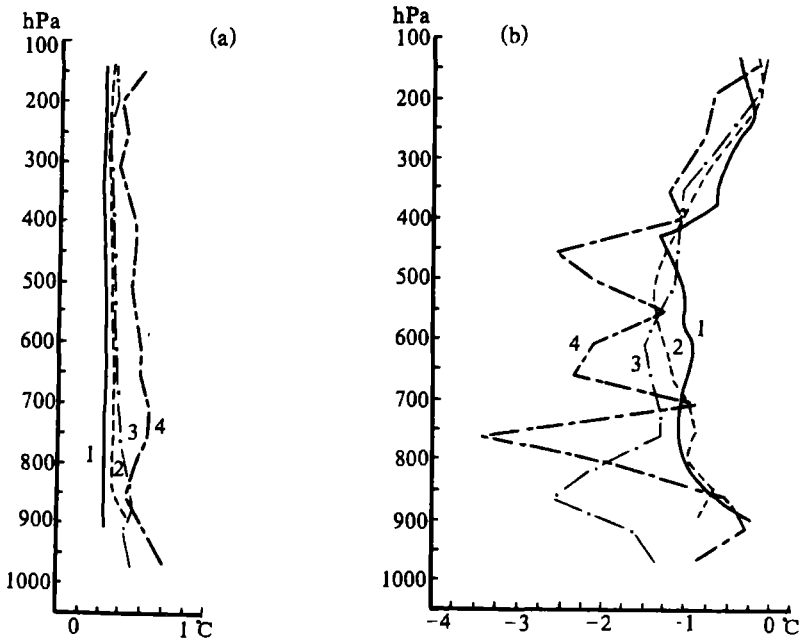


Fig. 7. Radiative heating and cooling (in  $^{\circ}\text{C}/\text{d}$ ): (a) shortwave heating in winter, (b) longwave cooling in winter.

the maximum value, which is located near 700 hPa, reaches  $2^{\circ}\text{C}/\text{d}$ . Slight decrease of moisture is found in the boundary layer which may be the result of upward transport of moisture by turbulence activity. The most powerful moistening is reached in Box 2; while in Box 3, this process tends to become weaker. It is in accordance with the result of land-air latent heat turbulent exchange given in the previous section. There is a point to pay more attention in Box 4 where the distribution curve shows a large increase of moisture. It can be inferred from the structure analysis of moisture in cold high given in the previous section that this phenomenon may result mainly from reevaporation of cloud layer or precipitation under stable stratification. The reevaporation of cloud or precipitation can result in local moistening.

Among three components of the apparent heat source, which are radiative heating, sensible heating and condensation heating, radiative heating exerts some effect, especially in winter when the condensation process is very weak and sensible heating is limited in boundary layer and upper layer of the troposphere. So the radiative heating (or cooling) will play a relatively important role in heat balance. To understand further the effect of radiation process on atmospheric heat balance, we calculate the distributions of radiative heating or cooling (See Fig. 7). In winter, cold air obtains a small amount of solar radiation in Box 1. As the cold air moves southward, the solar radiation has more and more effect on heating atmosphere. In Box 3, the solar radiation heating is about  $0.5^{\circ}\text{C}/\text{d}$  which is much larger than that at early stages. Over the ocean, the solar radiative heating in full depth of the atmosphere increases to  $0.5\text{--}1^{\circ}\text{C}/\text{d}$ . The vertical distribution of longwave radiation in winter cold air has different features as its geographic location changes. In the source area and North China (Boxes 1 and 2), longwave radiation shows cooling effect in a thick layer where cooling rate is  $-1^{\circ}\text{C}/\text{d}\text{--}1.5^{\circ}\text{C}/\text{d}$ . In Box 3, an obvious radiative cooling layer appears in the lower layer. From its location below the

middle layer inversion, we may infer that it may be related to top of low cloud just under the inversion. In Box 4, three relatively strong peaks of longwave radiative cooling arise at 750, 650 and 450 hPa, respectively. It can be seen by comparing quantities of longwave radiation in four different subdivisions that the radiative cooling is enhanced when the cold high moves to South China or the sea region,  $-2$ — $-3$  °C / d of cooling rate in Box 4, for example. These results are in agreement with the radiation cooling rate under unperturbed atmosphere given by Albrecht and Cox (1975).

Solar radiation heating is much more significant in summer than in winter. There is a large heating ( $1$ — $2$ °C / d), especially in the lower troposphere. The distributions of longwave radiation change a lot in vertical direction, but they have a general tendency of two strong cooling layers in the lower and upper troposphere and a weak cooling layer in between. The radiation cooling rates in Boxes 2 and 3 of four regions are larger (figure is omitted).

Through the above analysis, it can be seen that the longwave radiation cooling is an important component of heat source in winter, while the importance of shortwave radiation arises clearly in summer, especially in the layer near the surface.

## VI. CONCLUSIONS

In the present paper, 8 cases of strong cold air activities in different seasons of 1981 are selected and structures and heat balance of cold highs at different stages are discussed in more detail. We have paid a lot of attention to calculating the sensible and latent heat turbulence exchanges occurring at land-air interface over China from a relatively complete data set of surface observation by using similarity theory. We have also computed turbulence diffusion processes, radiation processes and apparent heat source and apparent moist sink by using upper-air sounding data. Through these analyses, we have obtained the following results about structure and physical transformation of the Siberian high:

(1) There are two kinds of inversions in winter cold high. One is near the surface and mainly in source area and North China which is connected with strong longwave radiation of surface and the lower atmosphere. However, as the cold high moves southward further, this kind of inversion disappears. The other kind of inversion or isothermal layer develops in the middle troposphere which may be created by large-scale downdraft heating. In summer, low stability and strong turbulence activity make inversion inside cold high difficult to form and to maintain.

(2) Cold air transformation in temperature and humidity starts just after its departing from its sources area. In winter, the transformation is intensified as cold high moves southward and the most violent phase is reached over the warm sea surface. In summer, the maximum changes appear in Mongolia and North China.

(3) According to upward turbulent heat transport near the surface, transformation is obviously stronger in summer when total heat flux can reach  $426 \text{ W m}^{-2}$  than in winter. Sensible heating is a main factor in transformation on land. In summer, the amount of latent heat transport may be the same or even larger than that of sensible heat transport and the strongest upward transport processes of sensible heat and latent heat all occurred in North China.

(4) It is indicated by calculations of the surface turbulence flux which have 4 observation times each day that the physical processes occurring in the lower troposphere have remarkable diurnal variation. Not only quantities of flux have larger difference, but also directions of flux may be reverse. So it can induce large error or even give misunderstanding if only daily mean

data or 08 BT and 20 BT data are used in computation. In winter cold air activities, mean momentum drag coefficient is  $5.5 \times 10^{-3}$  and mean total heat flux is  $75 \text{ W m}^{-2}$  in North China, and  $5.9 \times 10^{-3}$  and  $84 \text{ W m}^{-2}$  respectively in the central and South China. In summer, corresponding values are  $6.6 \times 10^{-3}$  and  $251 \text{ W m}^{-2}$  in North China and  $7.7 \times 10^{-3}$  and  $172 \text{ W m}^{-2}$  in the central and South China. These values are less than  $256 \text{ W m}^{-2}$  obtained during AMTEX'74 (Ninomiya, 1977), but they are unneglegible after all.

(5) For winter cold high, the ocean is the region where is the last stage of its transformation and is also the most violent phase. However, for summer cold high, because it has undergone a thorough transformation, the air mass does not continue to increase in temperature and in humidity, on the contrary, its temperature and humidity both show a decreasing tendency when it travels to ocean.

(6) The turbulence diffusion coefficients of the atmosphere above the surface layer indicate that there are two strong turbulent activity layers from the surface to 100 hPa inside cold air. One is in the planetary boundary and the other is located near the jet stream. The existence of the two strong turbulent activity layers, especially the upper one, can be felt by studying heat budgets. It implies that clear-air turbulence may play a some part in heat balance of cold high.

#### REFERENCES

- Albrecht, B. and Cox, S. K. (1975), The large-scale response of the tropical atmosphere to cloud-modulated infrared heating, *J. Atmos. Sci.*, **32**: 16—24.
- Businger, J. A., Wyngaard, J. C., Izmmi, Y. and Bradly, E. F. (1971), Flux-profile relationships in the atmospheric boundary layer, *J. Atmos. Sci.*, **28**: 181—189.
- Ding Yihui (1987), *Diagnostic Methods in Synoptic Dynamics*, Science Press, Beijing (in Chinese).
- Ding Yihui and Krishnamurti, T. N. (1987), Heat budgets of Siberian high and the winter monsoon, *Mon. Wea. Rev.*, **115**: 2428—2449.
- Lenchow, D. H. and Agee, E. M. (1976), Preliminary results from the air mass transformation experiment (AMTEX), *Bull. Amer. Meteor. Soc.*, **57**: 1346—1355.
- Louis, J-F. (1979), A parameteric model of vertical eddy fluxes in the atmosphere, *Bound. Layer Meteor.*, **17**: 187—202.
- Ninomiya, K. (1977), Heat energy budget of the polar air mass transformation over Kuroshio region under the situation of strong subsidence, *J. Meteor. Soc. Japan*, **55**: 431—441.
- Nitta, T. and So, S.S.(1980), Structure and heat, moisture and momentum budgets of a convective mixed layer during AMTEX'75, *J. Meteor. Soc. Japan*, **58**: 378—393.
- Pielke, R. A. (1981), Mesoscale numerical modelling, *Advances in Geophysics*, **23**: 185—344.
- Shapiro, M. A. (1976), The role of turbulent heat flux in the generation of potential vorticity in the vicinity of upper-level jet streams, *Mon. Wea. Rev.*, **102**: 892—906.
- Yeh Tucheng and Gao Youxi et al. (1981), *Meteorology on the Tibetan Plateau*, Science Press, Beijing (in Chinese).